ORIGINAL PAPER

Numerical Simulation on Cross-Layer Propagation of Hydraulic Fracture in Sand–mud Interbedded Layers: Taking the Shahejie Formation in BZ 25–1 Offshore Oilfield as an Example

Xu Guo[1,2] · Haiyan Zhu[1,2] · Peng Zhao[3] · Hu Jiang[4] · Guangai Wu[4] · Lei Tao[1,2] · Chao Liu[1,2] · Shijie Chen[1,2] · Jinghua Chen[1,2]

Abstract

The low-porosity, ultra-low-permeability tight sandstone oil and gas reservoirs are characterized by extensive reserves and widespread distribution, thus holding significant promise for exploration and development. In the Bohai Bay Basin, the Bozhong 25–1 (BZ25-1) oilfield presents a geological characteristic where sand–mud interbeds vertically develop within the third member of the Shahejie Formation (Es_3). However, the previously employed hydraulic fracturing conditions, characterized by 'low injection rates and high fluid viscosity', encountered difficulties in achieving effective cross-layer propagation of hydraulic fractures, consequently yielding suboptimal outcomes in terms of fracturing modifications. At present, the integrated offshore hydraulic fracturing vessels have gradually entered the development of offshore oil fields, which has improved the pumping capacity of offshore fracturing and can significantly improve the fracturing effectiveness. Therefore, this paper has established multiple sets of three-dimensional fluid–solid coupled finite element models, verifies the reliability through physical simulation experiments, and analyzes the rules of fracture cross-layer propagation from both geological and engineering perspectives. The results indicate that: (1) Increasing the injection rate can directly improve the vertical propagation capability of hydraulic fractures while also affect the length of the fractures. (2) The increase of viscosity will make it easier for hydraulic fractures to pass through the barriers. Once a specific viscosity threshold is exceeded, as the viscosity continues to increase, there is no longer a significant change in the injection volume of fracturing fluid required for fracture propagate through interlayers and the change in fracture geometry becomes less pronounced. (3) Variations in the minimum horizontal principal stress differential between layers notably impact the cross-layer propagation capability, leading fractures to preferentially propagate within layers characterized by lower stress. (4) The increase of reservoir thickness results in an expanded fracture area within the target reservoir, subsequently influencing the effect of fracture propagation across layers. The conclusions drawn from this study can provide theoretical guidance for the extensive hydraulic fracturing development of the Es_3 in BZ25-1 region.

Extended author information available on the last page of the article

Highlights

- With the improvement of fracturing conditions in offshore oil fields by offshore hydraulic fracturing vessels, this paper investigates the vertical propagation of hydraulic fractures in the sand–mud interbedded reservoirs of the third member of Shahejie Formation in BZ25-1 offshore oilfield.
- A multiple interbedded physical simulation rock sample is prepared and subjected to hydraulic fracturing experiment through the triaxial large-scale physical simulation experimental system, thereby validating the numerical methods.
- The seepage–stress–damage coupled mathematical model is employed to establish multiple three-dimensional fluid–solid coupling finite element models representative of sand–mud interbedded formations.
- By varying the interlayer thickness and the altering geological conditions or engineering factors, this paper analyzes the propagation patterns of hydraulic fractures within interbedded rock formations.

1 Introduction

Tight oil and gas, as a major unconventional energy resource, have now become a crucial component of the world's hydrocarbon reserves. The estimated total global resources of tight gas are approximately 210×10^{12} m^3, with China contributing around 10% to the world's resources base (Wei et al. 2017; Sun et al. 2019; Jia et al. 2022). The efficient development of the tight resources has emerged as a focal point of research for scholars worldwide. Tight sandstone reservoirs are typically characterized by low permeability, low porosity, and significant heterogeneity, making conventional development methods economically inefficient. Hydraulic fracturing technology is the primary approach to enhance productivity in low-permeability oil and gas reservoirs (Zhu et al. 2016). Sand–mud interbeds are common formation type within such reservoirs. When conducting hydraulic fracturing operations in tight sandstone reservoirs containing both upper and lower mudstone layers, it becomes essential to predict the vertical extension extent of hydraulic fractures and their propagation across layers, thereby optimizing the on-site hydraulic fracturing construction design. The Es$_3$ reservoir in the Bozhong area is characterized by its tight nature and significant three-dimensional stress differences (Wang et al. 2016; Song et al. 2020). This reservoir features vertical development of sand–mud interbeds with non-uniform mudstone interlayer thickness. The hydraulic fractures are obstructed by these mudstone layers, making it challenging for them to propagate through the interlayers and resulting in suboptimal fracturing outcomes. To increase production capacity, there is an urgent need to conduct an in-depth study on the vertical propagation behavior of hydraulic fractures.

In the past decade, global discoveries of large oil and gas fields have seen a significant increase, with over 80% of these discoveries being offshore. China's marine oil and gas resources hold immense potential for exploration and development, and the Bohai Sea region stands as one of the primary areas for offshore petroleum production in China. Compared to onshore oilfields, offshore oil fields often face challenges in providing adequate conditions for hydraulic fracturing. Taking Bozhong area as an example, hydraulic fracturing on offshore platforms is typically conducted with a "low injection rate and high viscosity" approach (with an injection rate of around 4 m^3/min and a fracturing fluid viscosity of approximately 200 mPa·s), resulting in suboptimal fracture cross-layer effect. At present, China is actively developing mobile fracturing equipment to enhance offshore fracturing capabilities. The introduction of offshore hydraulic fracturing vessels has improved the fracturing practices in offshore oil fields by increasing the pumping capacity for hydraulic fracturing fluids on offshore platforms, resulting in more effective expansion and extension of hydraulic fractures (Fan et al. 2021). The promising development prospects and trends of offshore hydraulic fracturing vessels are conducive to further offshore oil and gas exploitation. Therefore, it is necessary to conduct further study on the fracture extension under improved fracturing conditions.

In the hydraulic fracturing process for interbedded reservoirs, understanding the vertical extension of hydraulic fractures is of paramount importance (Gu and Siebrits 2008; Fisher and Warpinski 2012; Xu et al. 2019 Pandey et al. 2021). During on-site fracturing operations, multiple uncontrollable factors contribute to the difficulty of predicting the vertical extension of hydraulic fractures, often stemming from variations in the mechanical properties and formation conditions between different lithological layers (Lu et al. 2015; Shel et al. 2017; Zhao et al. 2018). Regarding engineering factors, pumping rate and fracturing fluid viscosity directly affect the extension of hydraulic fractures (Wu et al. 2017; Tang et al. 2023). According to the current research, high pumping rates and high fracturing fluid viscosity can enhance the vertical extension

of hydraulic fractures along the fracture height, making it more favorable for fractures to propagate through the interlayers (Guo et al. 2017; Zhang et al. 2021, 2023). In view of the layer-crossing behavior of hydraulic fractures, some scholars have carried out a large number of numerical simulation studies based on physical simulation experiments, established vertical layer-crossing propagation models of hydraulic fractures (Xu et al. 2015; Yang et al. 2021), and summarized the law of partial layer extension of hydraulic fractures. Among all influencing factors, differences in interlayer stress are identified as the primary restricting factors for the height of hydraulic fractures (Warpinski et al. 1982; Eekelen 1982; Jeffrey et al. 1992; Huang et al. 2016). Wang et al. (2021) conducted a physical modeling experiment to investigate the cross-layer propagation in sandstone reservoirs. They supplemented their study by employing a two-dimensional finite element method to simulate the propagation of fractures through interlayers. Fu et al. (2022a) by combining the results of physical model experiment and numerical model, concluded that the ratio between interlayer differences in horizontal stress and interlayer thickness is the primary controlling factor affecting the vertical expansion of fractures. Simonson et al. (1978) analyzed the influence of the mechanical property differences between producing layers and interlayers on the vertical expansion of hydraulic fractures. Warpinski et al. (1981), Teufel et al. (1984), Adachi et al. (2010) and Chitrala et al. (2013) individually investigated the impact of in situ stress on the expansion morphology of hydraulic fractures in stratified formations using theoretical and experimental approaches. Yue et al. (2019) explored the effects of interlayer differences in elastic modulus on the height of fractures in stratified oil reservoirs. Fu et al. (2022b) conducted research on shale formations to study the influence of pumping rate and fluid viscosity on the vertical expansion of hydraulic fractures.

In summary, the vertical propagation of hydraulic fractures is primarily influenced by engineering factors and geological conditions. Previous studies have often focused on analyzing fracture expansion using individual parameters, and have neglected the coupling effects of changes in interlayer thickness on the vertical propagation of fractures. When employing a two-dimensional simulation approach, the model tends to overlook the extension process of the fracture length, resulting in excessive extension of fracture height and thereby yielding less accurate results. Based on observed hydraulic fracture results from field operations and considering that the difference between vertical stress and minimum horizontal principal stress exceeds 30 MPa in the Bozhong area, making it difficult for horizontal fractures to form, this paper overlooks the impact caused by sand–mud interbed interfaces (Huang et al. 2017; Khisamitov and Meschke 2018; Zhou
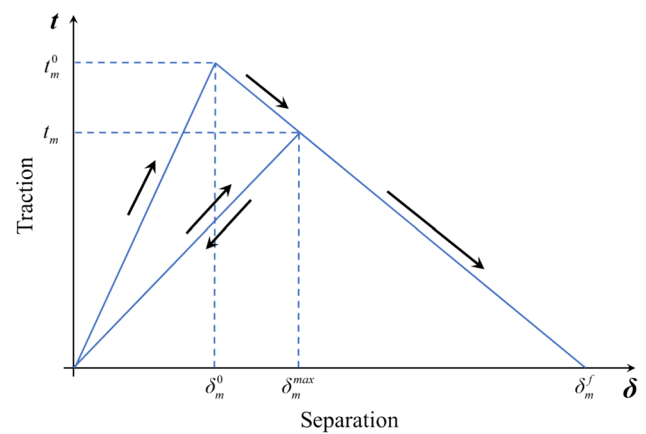

Fig. 1 The traction–separation criterion for cohesive element

et al. 2022) to explore the vertical extension of fractures. To address the current construction scale of offshore hydraulic fracturing vessels and investigate the fracture propagation through interlayers under the conditions of "large pumping rate and low viscosity fluid" in the target area, this paper utilized the cohesive zone method (CZM) to establish multiple sets of three-dimensional numerical models for fracture propagation. Using multiple sets of barrier thicknesses as basic variables, a fracturing simulation study was systematically conducted taking into account the effects of engineering parameters (pumping rate and viscosity) and stratigraphic parameters (the minimum horizontal principal stress differential between layers and reservoir thickness). The study methodology not only enhances comparability among results but also enables predictive analysis of hydraulic fracture propagation morphology through cross-comparative analysis, facilitating a deeper exploration of the cross-layer propagation patterns of hydraulic fractures. The findings of this study provide theoretical references for the development of hydraulic fracturing operations in tight sandstone reservoirs in the Bozhong 25–1 oilfield.

2 Seepage-Stress-Damage Coupling Mathematical Model for Dynamic Propagation of Fractures

2.1 Damage Initiation and Evolution Mode of Cohesive Element

The geometric characteristics of hydraulic fractures are primarily characterized by cohesive element, and the propagation and extension of fractures are predominantly influenced by the mechanical properties of cohesive element. The cohesive zone model describes the force–displacement behavior

of the interface. As shown in Fig. 1, the damage mode of the cohesive element follows the T–S (Traction–Separation) criterion (Tomar et al. 2004; Dahi Taleghani et al. 2016), and the stress–strain relationship is assumed to exhibit linear elastic behavior, with the stress borne by the cohesive element serving as the damage criterion (Huang et al. 2022).

When the interface opening displacement is small, the interface exhibits elastic response. As the load increases, the interface opening displacement also increases accordingly. When the traction force reaches the tensile strength of the element, damage starts to occur, stiffness gradually degrades, and the load-bearing capacity of the element begins to decrease, exhibiting material softening characteristics until it decreases to 0, indicating complete failure of the material, and the load-bearing capacity becomes irrecoverable. Once the traction force linearly diminishes to zero, signifying full interfacial failure at a critical displacement, any subsequent reduction in stress or strain becomes irreversible. During unloading, the stress–strain response would follow a path along the slope indicated by the arrow, but ultimate return to the initial state is not implied.

In Fig. 1, t_m and t_m^0 are the actual stress borne by the element and the maximum stress it can withstand before damage, respectively. δ_m^{max}, δ_m^0, and δ_m^f are the maximum relative effective displacement during loading, the displacement at the beginning of damage, and the displacement when the element is completely damaged, respectively. It assumes that the material exhibits linear elastic behavior until the traction force reaches the tensile (shear) strength or the separation of the cohesive interface exceeds the damage initiation displacement.

The constitutive behavior of the cohesive element comprises linear elastic behavior, damage initiation, and damage evolution. The linear elastic stage when the element is not damaged can be defined by the elastic constitutive matrix (Xu et al. 2022):

$$t = \begin{Bmatrix} t_n \\ t_s \\ t_t \end{Bmatrix} = \begin{bmatrix} K_{nn} & K_{ns} & K_{nt} \\ K_{ns} & K_{ss} & K_{st} \\ K_{nt} & K_{st} & K_{tt} \end{bmatrix} \begin{Bmatrix} \varepsilon_n \\ \varepsilon_s \\ \varepsilon_t \end{Bmatrix} = K \cdot \varepsilon \tag{1}$$

where t is the nominal stress vector on the interface of cohesive element, which consists of the stress components t_n, t_s, and t_t in the normal, the first tangential, and the second tangential directions. K is the stiffness matrix for the elastic response of the cohesive element. The nominal stress is defined as the stress component at each integration point divided by the initial thickness of the cohesive element. The nominal strain can be expressed as the ratio of the traction displacement at the integral point of the cohesive element to its original thickness. The nominal strain consists of ε_n, ε_s, and ε_t, which can be calculated as $\varepsilon_n = \delta_n/T_0$, $\varepsilon_s = \delta_s/T_0$ and

$\varepsilon_t = \delta_t/T_0$, where T_0 is the initial thickness of the cohesive element, δ_n, δ_s, and δ_t are the traction displacements in the normal, first tangential, and second tangential directions of the cohesive element, respectively.

The cohesive element uses stiffness degradation to describe the damage evolution process of the element. The damage evolution model is:

$$t_n = \begin{cases} (1-D)\bar{t}_n, & \bar{t}_n \geq 0 \\ \bar{t}_n, & \bar{t}_n < 0 \end{cases}$$

$$t_s = (1-D)\bar{t}_s \tag{2}$$

$$t_t = (1-D)\bar{t}_t$$

where $\bar{t}_n$, $\bar{t}_s$, and $\bar{t}_t$ are the stress calculated by linear elastic deformation when the normal, the first and the second tangential directions of the cohesive element are all damaged. D is the dimensionless damage factor, with a value range of 0–1. $D = 0$ indicates that the material is not damaged, and $D = 1$ indicates that the material is completely damaged.

The damage factor D can be expressed as:

$$D = \frac{\delta_m^f \left(\delta_m^{max} - \delta_m^0 \right)}{\delta_m^{max} \left(\delta_m^f - \delta_m^0 \right)} \tag{3}$$

The deformation of the cohesive element is described as a mixed mode of normal and tangential simultaneous damage, so δ_m^{max} can be expressed as:

$$\delta_m^{max} = \sqrt{\langle \delta_n \rangle^2 + \delta_s^2 + \delta_t^2} \tag{4}$$
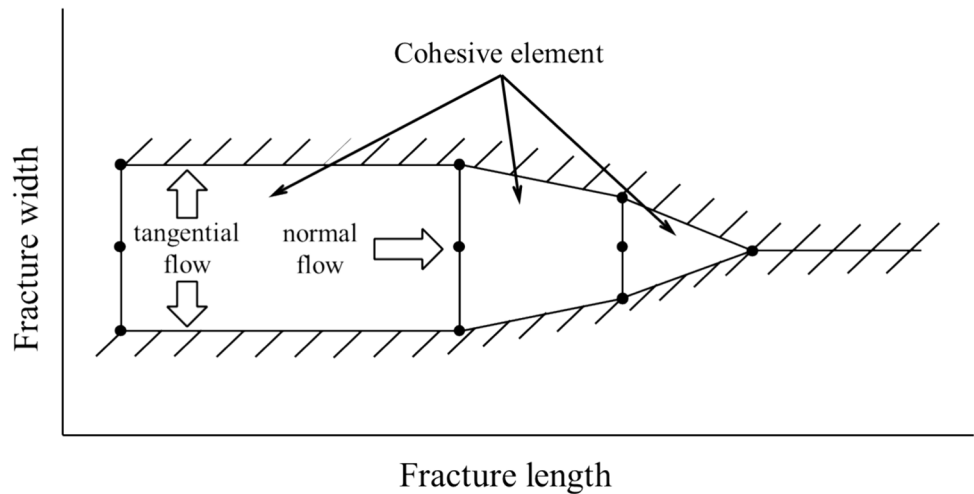
2.2 Fracture Propagation and Extension Criteria

When the mechanical conditions satisfy the damage initiation criterion, the cohesive element will be damaged according to T–S criterion. In this paper, the quadratic nominal stress criterion is used as the damage initiation criterion of cohesive element, and its expression is (Haddad et al. 2015)

$$\left(\frac{\langle t_n \rangle}{t_n^0} \right)^2 + \left(\frac{t_{s1}}{t_{s1}^0} \right)^2 + \left(\frac{t_{s2}}{t_{s2}^0} \right)^2 = 1 \tag{5}$$

where t_n is the normal stress of cohesive element; t_{s1} and t_{s2} are the shear stress in the first and second tangential directions of the cohesive element; t_n^0 is the tensile strength of cohesive element; t_{s1}^0 and t_{s2}^0 are the shear strength of cohesive element; $\langle \rangle$ is the Macaulay bracket, indicating that the cohesive element does not produce damage when subjected to compressive stress or compressive strain.

Fig. 2 Fluid flow in fracture (Zhu et al. 2023)

where E is the elastic modulus of rock; v is the Poisson's ratio of rock; K_{IC}, K_{IIC}, and K_{IIIC} are type I, type II, and type III fracture toughness, respectively.

2.3 Fluid Flow in Cohesive Element

Due to the significantly greater length of hydraulic fractures compared to their width, fluid flow within the fracture can be treated as one-dimensional. Figure 2 illustrates two modes of fluid flow within the fracture: radial flow along the length of the fracture and normal flow perpendicular to the radial flow. The latter is also referred to as fluid infiltration, representing the flow of fluid from the fracture into the rock pore. The fluid flow in fractures is divided into tangential flow and normal flow. Usually, the internal fluid is assumed to be incompressible Newtonian fluid, and the calculation formula of tangential flow is (Zhu et al. 2015).

$$q = -\frac{w^3}{12\mu}\nabla p \tag{11}$$

where q is the fluid flow in the fracture; w is the fracture width changing with the fracturing time; μ is the viscosity of the fracturing fluid; ∇p is the fluid pressure gradient along the length direction in the cohesive element.
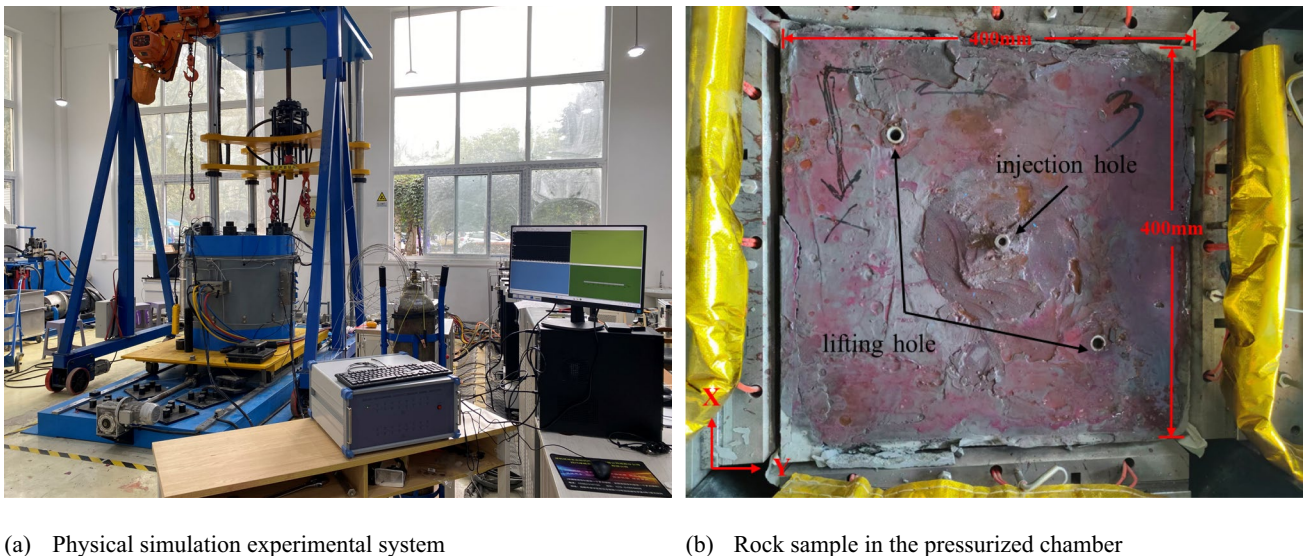
The equation describing the filtration of fracturing fluid is

$$\begin{cases} q_t = c_t(p_f - p_t) \\ q_b = c_b(p_f - p_b) \end{cases} \tag{12}$$

where p_t and p_b are the pore pressure at the upper and lower surfaces of the fracture; c_t and c_b are the filtration coefficient of the upper and lower surfaces; q_t and q_b are the normal volume flow of the upper and lower surfaces.

Total flow is

$$q_{\text{total}} = q_t + q_b, \tag{13}$$

$$\langle t_n \rangle = \begin{cases} t_n, & t_n \geqslant 0 \\ 0, & t_n < 0 \end{cases} \tag{6}$$

The cohesive element uses stiffness degradation to describe the evolution process of the element, and its expression is

$$T = (1 - D)\bar{T} \tag{7}$$

where $\bar{T}$ is the stress obtained by the current strain according to the stiffness before damage; T is the actual stress; D is the damage factor.

For mixed-mode fracture initiation, the BK mixed propagation model (Benzeggagh and Kenane 1996) is used, represented as

$$G_n^c + (G_s^c - G_n^c)\left(\frac{G_s + G_t}{G_n + G_s + G_t}\right)^\eta = G^c \tag{8}$$

where G_n, G_s, and G_t are the work done by the traction stress and its conjugate displacement in the normal, the first tangential and the second tangential directions respectively. η is the dimensionless constant associated with the properties of the material itself, taken in this paper as 2.284. The critical fracture energy G^c is the area enclosed by the T-S curve and the coordinate axis.

G_n^c, G_s^c, and G_t^c are the critical fracture energy required for the cohesive element to damage in the normal, the first tangential and the second tangential directions, respectively, which can be expressed by the following formula:

$$G_n^c = \frac{K_{IC}^2}{E}\left(1 - v^2\right) \tag{9}$$

$$G_s^c + G_t^c = \frac{K_{IIC}^2}{E}\left(1 - v^2\right) + \frac{K_{IIIC}^2}{2u} \tag{10}$$

(a) Physical simulation experimental system

(b) Rock sample in the pressurized chamber

Fig. 3 Experimental equipment and rock sample

The continuity equation of mass conservation is (Chen 2012)

$$\frac{\partial w}{\partial t} + \nabla q + \left(q_t + q_b\right) = Q(t)\delta(x, y) \tag{14}$$

where Q(t) is the time-dependent injection rate.

3 Experimental Verification

To verify the reliability of the established numerical model, a large-scale physical simulation experiment was conducted on the sand–mud interbedded formation. The experiment was conducted using the triaxial large-scale physical simulation experimental system of the State Key Laboratory of Oil & Gas Reservoir Geology and Exploitation at Chengdu University of Technology. The experimental system is shown in Fig. 3a.

The sand–mud interbedded rock sample was artificially made. The rock sample consisted of a 7-layer structure with alternating layers of mudstone and sandstone, with overall dimensions of $400 \times 400 \times 400$ mm. Sandstone and mudstone layers were cast using different pro-portions of cement, coarse sand, and fine sand to control the differences in rock mechanical properties between layers. As the elastic modulus of sandstone in actual formations is greater than that of mudstone, the ratio of cement to sand in sandstone layers is set at 1.8:1, while in mudstone layers, the ratio is set at 2:1. This reduction in the cement proportion aims to increase the elastic modulus of the rock layers. Experimental measurements showed an elastic modulus of 18.9 GPa for the sand layer and 15.5 GPa for the mud layer. The simulated

wellbore had dimensions with an outer diameter of 18 mm, an inner diameter of 8 mm, a length of 240 mm, and a perforation diameter of 2 mm. As shown in Fig. 3b, the stress values in the x, y, and z directions were set at 22 MPa, 19 MPa, and 30 MPa, respectively. The injection rate of fracturing fluid was controlled at 20–30 ml/min.

Based on the experimental result in Fig. 4a, it can be observed that the hydraulic fracture propagated vertically relative to the bedding planes. The experimental result exhibited a predominance of vertical fractures and an absence of horizontal fractures. Corresponding numerical simulation was conducted for the physical model experiment. Layer division, mechanical parameters, loads, and boundary conditions of the numerical model were set according to the aforementioned physical model experiment. As shown in Fig. 4b, the fracture propagation result obtained from the numerical simulation generally match the fracture extension region observed in the physical model experiment. Comparing the injection pressure curves of the two methods (Fig. 5), the experimental fracturing pressure is 22.4 MPa, while the numerical simulation yields 21.7 MPa, showing a difference of around 3%. The result of the numerical simulation was relatively consistent with the data from the experiment. Therefore, the established sand–mud interbedded hydraulic fracture propagation numerical model was determined to be reliable.
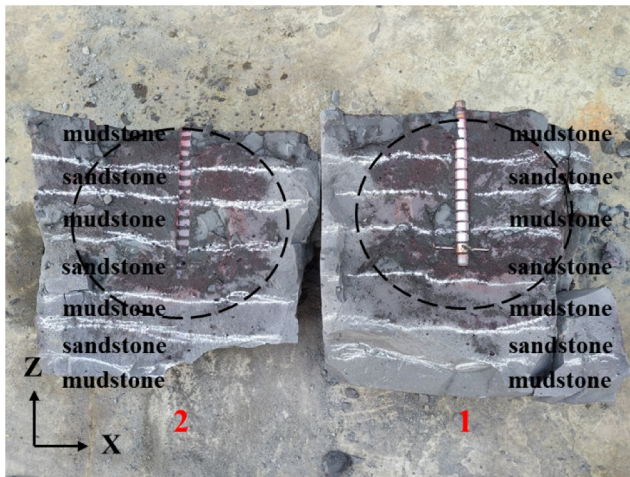
(a) Sectional drawing of the rock sample
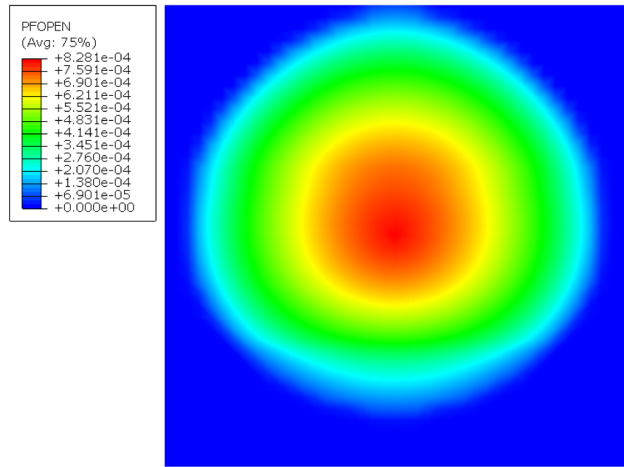
(b) The numerical simulation result corresponding to the experiment

Fig. 4 Experimental result and numerical simulation result
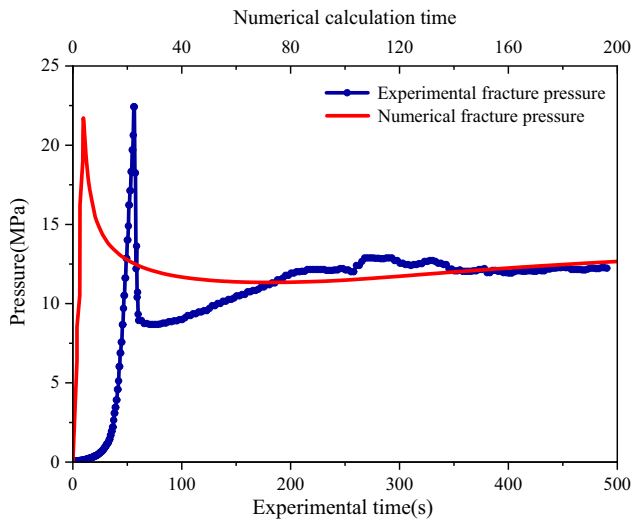

Fig. 5 Comparison of the field construction pressure curve and the numerical simulation outcome

4 Vertical Fracture Propagation Model for Sand–mud Interbedded Layers

To investigate the influence of engineering factors and geological conditions on the vertical propagation of hydraulic fractures in sand–mud interbedded layers, a comprehensive plan for simulating fracture propagation was developed. In consideration of practical field construction conditions and the working condition of offshore hydraulic fracturing vessels, a study framework was developed to investigate the impact of various factors on hydraulic fracture propagation within different thicknesses of mudstone interlayers in

Table 1 Types and values of variables in numerical simulation

Variable type	Value sets
Thickness of mudstone interlayer (m)	6 8 10 12
Injection rate (m³/min)	4 6 8 10
Viscosity of fracturing fluid (mPa·s)	10 50 100 300
Thickness of sandstone (m)	10 12 14 16
Minimum horizontal principal stress differential between layers (MPa)	-4 -2 0 2 4

sand–mud interbedded formations. Four key variable dimensions were considered: pumping rate, viscosity of fracturing fluid, reservoir thickness, and the minimum horizontal principal stress differential between layers. Multiple sets of numerical models were established to simulate their effects. The selection of viscosities and pumping rates considered the field construction practices involving slickwater and gelled fluid, as well as the operational capabilities of current offshore hydraulic fracturing vessels. The stratigraphic conditions were based on the actual situation of the Es_3 reservoir. The specific parameters of the numerical models are shown in Table 1. The baseline settings for the models include a pumping rate of 6 m³/min, a viscosity of 50 mPa·s, a minimum horizontal principal stress differential of 2 MPa, and a target reservoir thickness of 12 m.

4.1 Modeling

Based on the actual formation conditions of the study area, a three-dimensional fluid–solid coupling finite element model of 7-layer was established (Fig. 6a). S1, S2, and S3 are sandstone reservoirs. M2 and M3 are mudstone barriers. M1 and
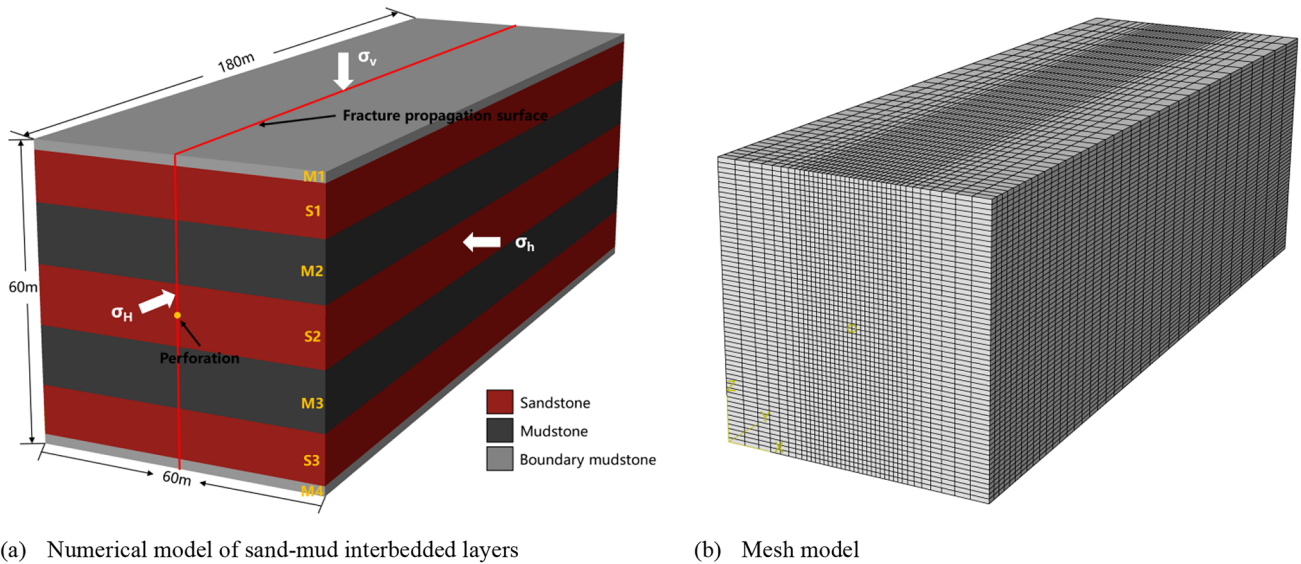
(a) Numerical model of sand-mud interbedded layers

(b) Mesh model

Fig. 6 Establishment of numerical model for fracture propagation
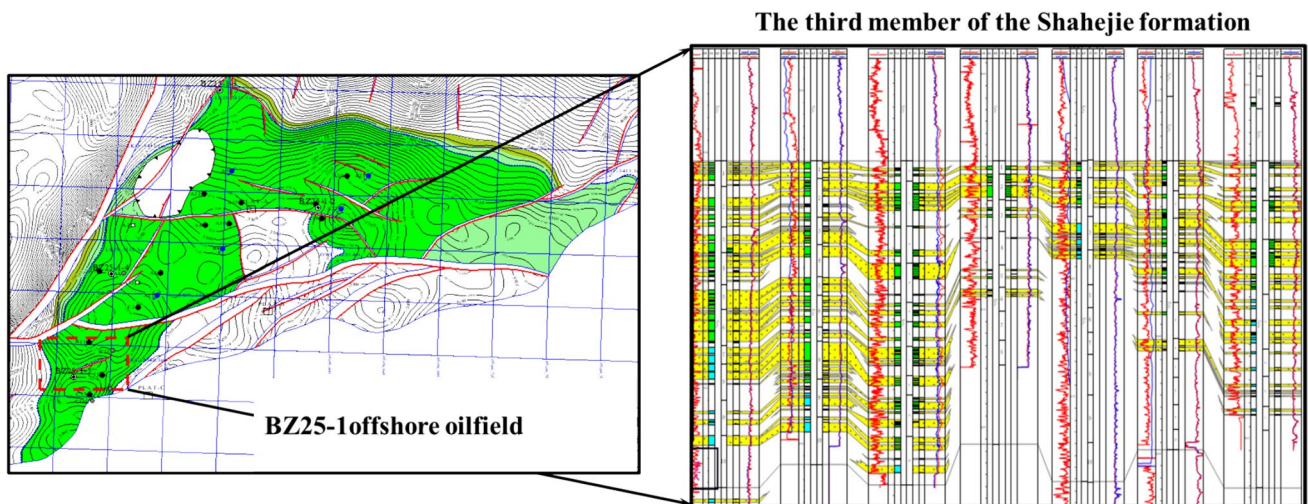

Fig. 7 The stratigraphic distribution characteristics of the third member of Shahejie formation in BZ 25–1 offshore oilfield

M7 were set as boundary interlayers, serving as constraints with material properties identical to M2 and M3. The total thickness of the model is 60 m, with a length (the extension direction of the fracture length) of 180 m and a width of 60 m. The model was divided into hexahedral elements, with predefined cohesive element fracture plane in the vertical direction at the perforation points to simulate the hydraulic fracture propagation path. Boundary conditions are established on the six faces of the model. Among them, the plane where the perforation point is located is set to have a mirror symmetry effect, while the displacement is constrained on the remaining five faces to simulate actual reservoir conditions. To obtain more accurate results, the grid was locally refined near the fracture propagation surfaces to enhance computational accuracy and convergence. The mesh type employs 8-node three-dimensional linear displacement pore pressure elements, the total number of model grids is 84,240, and the total number of nodes is 92,537. The meshing of the model is shown in Fig. 6b.

4.2 Parameter Settings

The vertical stress in the BZ25-1 Es_3 reservoir reaches over 87 MPa. The distribution of maximum and minimum horizontal principal stresses falls within the ranges of 65 MPa–70 MPa and 57 MPa–60 MPa, respectively. As
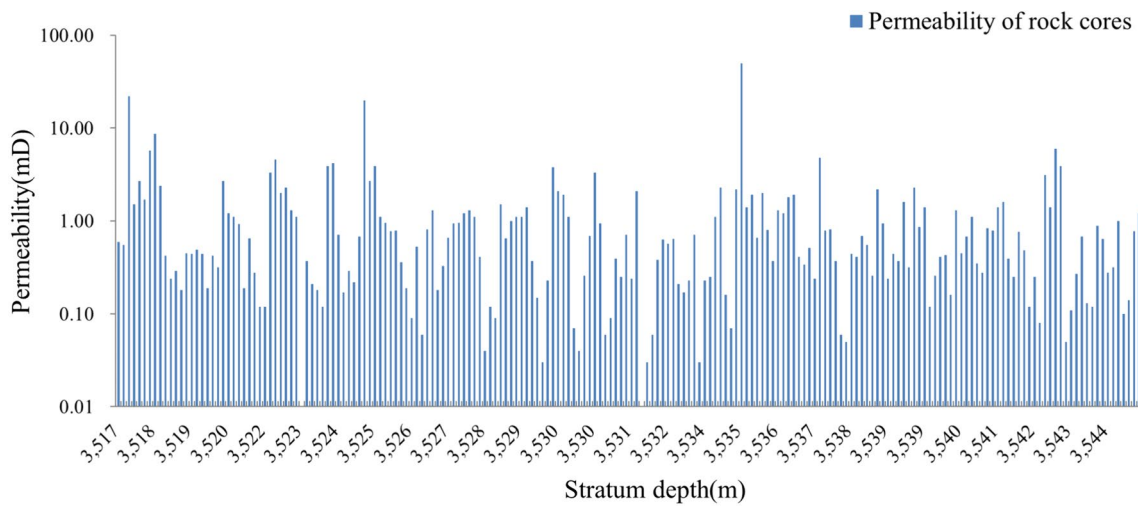
Fig. 8 Partial rock samples

**Fig. 9** Permeability statistics of rock cores at different depths

shown in Fig. 7, the third member of Shahejie formation exhibits alternating patterns of sandstone and mudstone layers in the vertical direction. Core samples were obtained from the target formation interval (Fig. 8). Uniaxial compression tests revealed that the sandstone exhibited uniaxial compressive strengths ranging from 27 to 38 MPa, while the mudstone exhibited strengths ranging from 34 to 42 MPa. As depicted in Fig. 9, the permeability was determined to have an average value of 1.9 mD based on 196 core samples collected at various depths. The average porosity of the reservoir segment is 12.5%. Considering the rock mechanical properties of the reservoir and the magnitudes of the three principal stresses, both the thickness of the sand–mud interbedded layers and the stress settings were determined based on the actual stratigraphic conditions of the target area. The specific parameters of the model are listed in Table 2.

4.3 Validation of Field Construction Practice

To validate the numerical simulation method, a comparison was made with field fracturing result. Well C-25, a vertical well in the BZ25-1 oilfield, was selected for numerical simulation. This well has undergone fracturing operations in the Es_3 reservoir. The C-25 well has a reservoir depth ranging from 3672.8 to 3831.5 m, with a net pay thickness of 56.9 m, permeability ranging from 1.8 to 3.7 mD, and porosity between 14.4% and 17.1%. Considering the distribution of sand–mud interbeds in well C-25, a single well numerical model was established to compute the pressure variation over time at the perforation point depicted in Fig. 10. This was then compared with the pressure curve obtained from the actual fracturing operation. Due to the influence of various factors during the hydraulic fracturing process, the construction

Table 2 Model parameter settings

Rock type	Young's modulus (GPa)	Poisson's Ratio	Permeability (mD)	Porosity (%)	Pore pressure (MPa)	Minimum horizontal principal stress (MPa)	Maximum horizontal principal stress (MPa)	Vertical Stress (MPa)	Tensile strength (MPa)	Shear strength (MPa)
Mudstone	15.4	0.165	1.2	9.8	35.5	58.8	68.8	91.2	3.8	18.6
Sandstone	17.2	0.192	3.8	13.8	35.5	56.8	66.4	91.2	3.2	15.7
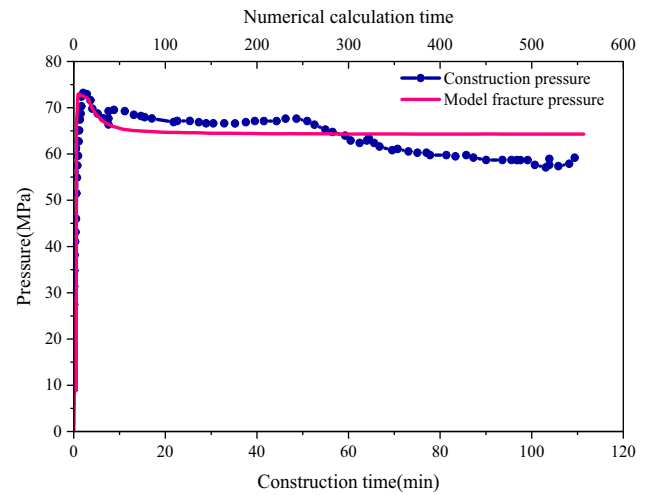
Fig. 10 Comparison of construction pressure curve and numerical simulation results

pressure curve exhibited some irregular fluctuations. The actual fracturing pressure was 73.49 MPa, whereas the simulated fracturing pressure was 72.56 MPa. Upon comparison, the model's fracture pressure was within 2% of the error compared to the on-site hydraulic fracturing. Following fracturing initiation, both exhibited a similar trend of pressure decline. This comparison validates the accuracy of the numerical model used in this study at the field level.

5 Results

This section primarily conducts a comparative analysis of hydraulic fracture propagation in terms of fracture height, width, and length. During the result analysis, real-world fracturing conditions are considered, and the simulation results with a half-fracture length of 180 m (reaching the model boundary) are chosen as the criterion to determine whether the fracture can pass through the interlayer. If it has not passed through the mudstone interlayer, it is considered as incapable of cross-layer propagation. Due to the numerous simulation results in this section, the fracture extension results for the 8 m-thick mudstone interlayer are selected to represent the extension of hydraulic fractures in the direction of fracture length.

5.1 Effect of Pumping Rate on the Vertical Propagation of Hydraulic Fracture Through Interlayers

In the BZ25-1 sandstone reservoir, on-site fracturing operations generally provide a pumping rate of 4 m³/min or less. This limitation severely restricts the height growth of
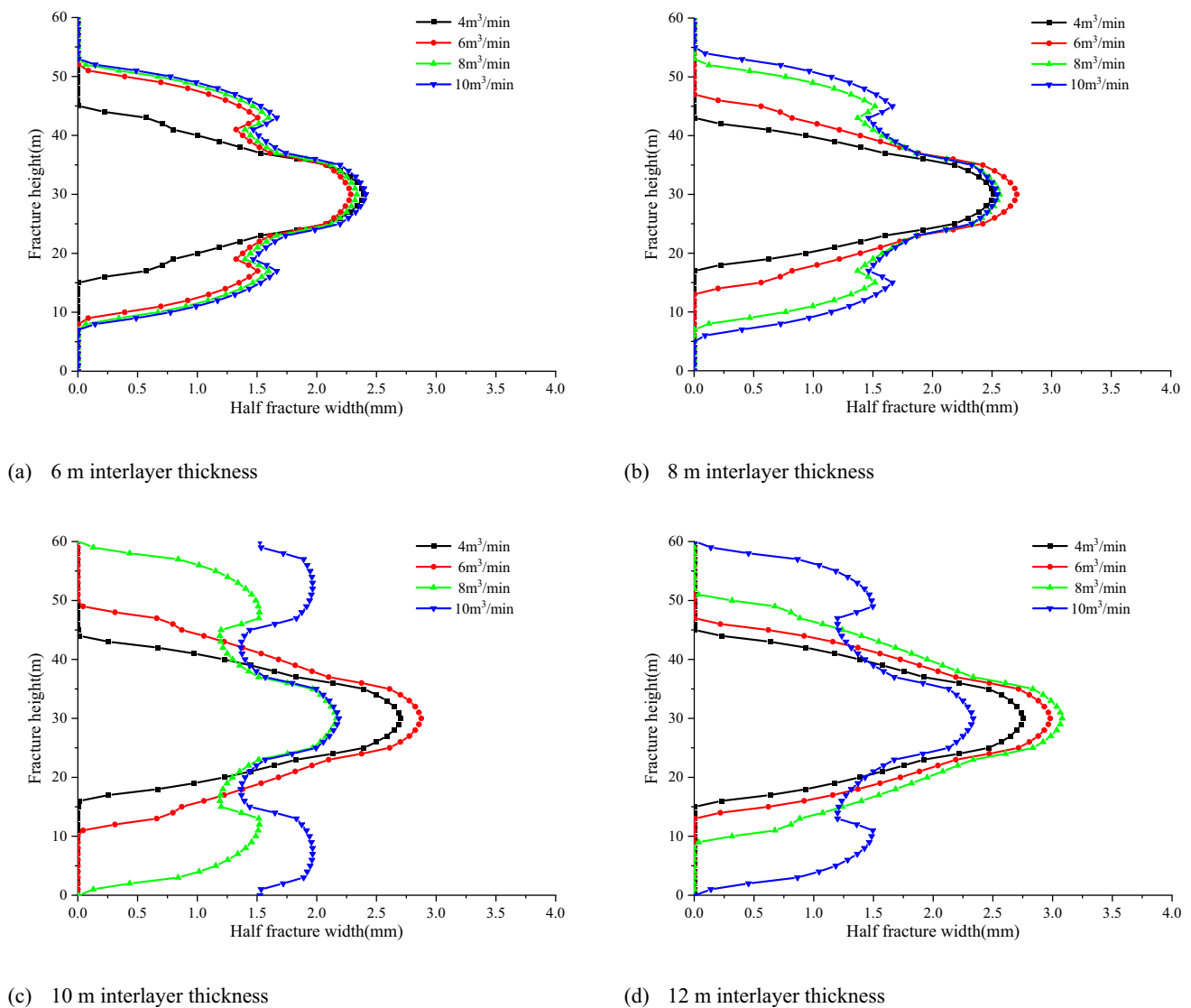
(a) 6 m interlayer thickness

(b) 8 m interlayer thickness

(c) 10 m interlayer thickness

(d) 12 m interlayer thickness

Fig. 11 The results of hydraulic fracture propagation through layers with varying injection rates under different interlayer thicknesses

hydraulic fractures, preventing them from passing through mudstone layers. The introduction of offshore fracturing vessels has significantly increased the pumping capacity for offshore fracturing operations. Therefore, in this section, we conducted simulations with different injection rates (Q) set at 4 m³/min, 6 m³/min, 8 m³/min and 10 m³/min to investigate the hydraulic fracture propagation through interbedded sand–mud layers after increasing the pumping rate. To ensure that the pumping rate is the sole influencing factor, the injection volume for each group of models is controlled to be identical. In each plot, the volume of fracturing fluid is uniformly set to the maximum required for propagating through the interlayer under different pumping rate conditions (consistent with other sections), allowing for the analysis of different fracture outcomes resulting from the same injection volume.

When the interlayer thickness is 6 m (Fig. 11a), the hydraulic fractures can propagate through the upper and lower interlayers when Q > 4 m³/min. Notably, the required injection volume for hydraulic fracturing is maximum when Q = 4 m³/min. The differences in fracture width between Q = 6, 8, 10 m³/min are relatively small, with half-width differences within 0.15 mm. As the interlayer thickness increases to 8 m (Fig. 11b), hydraulic fractures at Q = 4 m³/min cannot pass through the interlayer, and the variations in fracture width become more pronounced for Q = 6, 8, 10 m³/min. When the interlayer thickness enlarges to 10 m (Fig. 11c), hydraulic fractures under a pumping rate of 6 m³/min can achieve cross-layer propagation. At this point, hydraulic fractures at a pumping rate of 8 m³/min have already reached the boundary interlayers M1 and M4, and hydraulic fractures at a pumping rate of 10 m³/

(a) 4 m³/min

(b) 6 m³/min
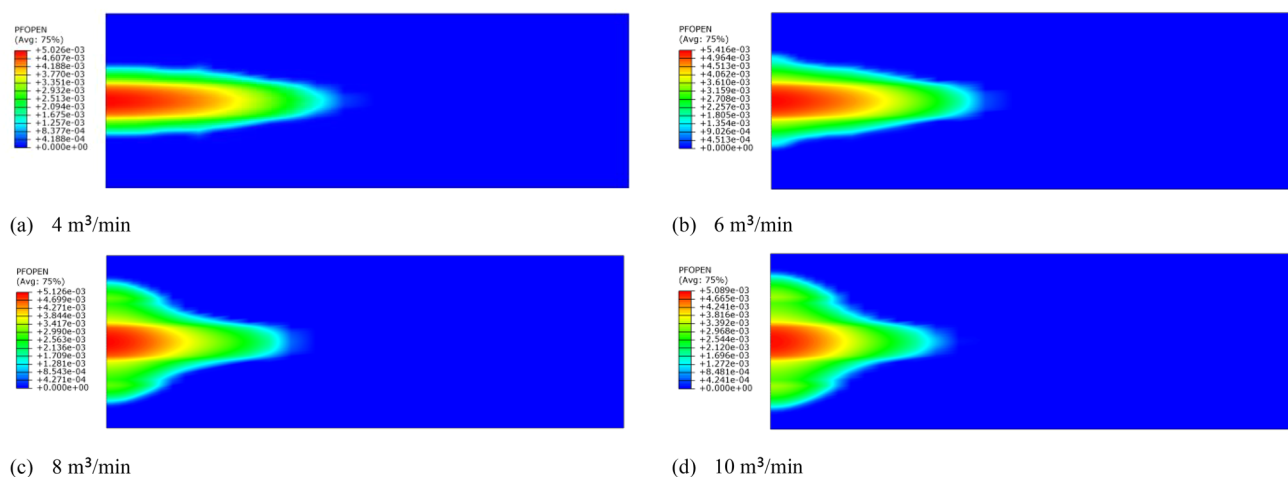
(c) 8 m³/min

(d) 10 m³/min

Fig. 12 The extensions of fracture length when the interlayer is 8 m under different pumping rates

min have passed through the boundary interlayers. When the barrier thickness rises to 12 m (Fig. 11d), the hydraulic fractures with $Q = 4.6$ m³/min are unable to cross the barriers of the target reservoir, while the hydraulic fractures with $Q = 10$ m³/min have reached the boundary interlayers.

Overall, the increase in interlayer thickness results in the need for higher pumping rates and greater injection volumes to achieve cross-layer propagation, leading to an overall increase in the fracture width. After the interlayer thickness increases to a certain level, lower pumping rates are insufficient to enable hydraulic fractures to propagate through the interlayer. Increasing the pumping rate not only significantly enhances the fracture's ability to propagate through the interlayer but also reduces the required injection volume. With the injection volume held constant, higher pumping rates may even result in secondary cross-layer fracture propagation.

From the expansion of hydraulic fractures along the fracture length, as depicted in Fig. 12, it is evident that when the pumping rate is low, insufficient pressure within the fracture hinders the hydraulic fracture from obtaining adequate energy to pass through the interlayer vertically. Consequently, the hydraulic fracture is constrained by the interlayer and can only propagate along the length of the reservoir. However, when the pumping rate is sufficient for hydraulic fracturing to pass through the interlayer, a higher rate favors vertical expansion, resulting in a shorter fracture length.

5.2 Effect of Fracturing Fluid Viscosity on the Vertical Propagation of Hydraulic Fracture Through Interlayers

In situations where pumping capacity is limited, hydraulic fracturing operations in the Es_3 reservoir typically utilize high-viscosity fracturing fluids, approximately 180 mPa·s, to enhance the fractures' propagation capability. With the ongoing advancements in offshore fracturing equipment, "large injection rate and low fluid viscosity" has gradually been incorporated into offshore oil field fracturing practices. To investigate the impact of changing fluid viscosity on cross-layer propagation of hydraulic fracture, viscosity levels of 10 mPa·s, 50 mPa·s, 100 mPa·s, and 300 mPa·s were selected for the study. To better illustrate the impact of fracturing fluid viscosity on fracture propagation, the viscosity difference is amplified. Given the notable influence of viscosity changes on fracture propagation through interlayers, this section presents curve plots based on four sets of viscosity conditions to analyze the effect of interlayer thickness variation on fracture propagation outcomes under different viscosity scenarios (while other sections are based on four sets of interlayer thickness).

When the fracturing fluid viscosity is 10 mPa·s (Fig. 13a), the hydraulic fracture cannot propagate through the 6 m interlayer, resulting in consistent fracture geometry regardless of the varying interlayer thicknesses. Under this viscosity condition, the fractures exhibit a narrower width, and the fracture height is restricted by the interlayer, with the fracture primarily extending along its length. With an increase in fracturing fluid viscosity to 50 mPa·s (Fig. 13b), hydraulic fractures can pass through interlayers with thicknesses of 6 m, 8 m, and 10 m but remain restricted by the 12 m interlayer. Notably, the injection volume of fracturing fluid required for the fracture to pass through the 10 m interlayer allows the fracture's height within the 6 m interlayer to reach the boundary interlayer. Once the fracturing fluid viscosity reaches 100 mPa·s (Fig. 13c), hydraulic fractures can pass through interlayers ranging from 6 to 12 m in thickness.

The curves illustrate that with decreasing interlayer thickness, hydraulic fractures exhibit narrower widths within the
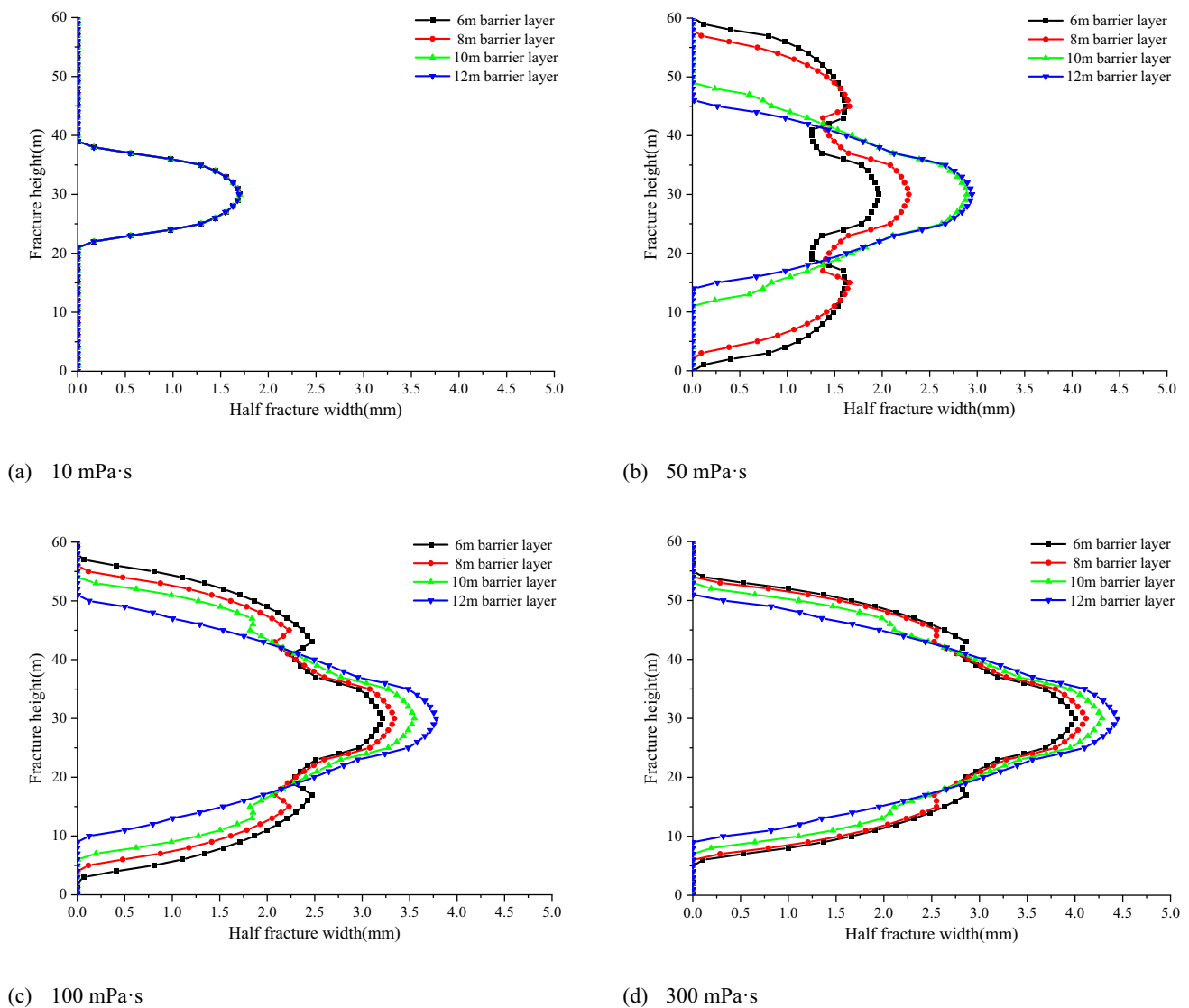
(a) 10 mPa·s

(b) 50 mPa·s

(c) 100 mPa·s

(d) 300 mPa·s

Fig. 13 The results of hydraulic fracture propagation through layers with varying interlayer thicknesses under different viscosities

M2, S2, and M3 layers while displaying wider widths inside the S1 and S3 layers, accompanied by an overall increase in fracture height. This is attributed to the reduced interlayer thickness, which requires a smaller injection volume for hydraulic fracture passing through the interlayers, making it easier for hydraulic fractures to access the upper and lower reservoir layers. Due to variations in the material properties and stress conditions of the reservoir and interlayer, fractures tend to propagate predominantly within the reservoir layers. Consequently, when the interlayer thickness is reduced, fractures are more likely to achieve cross-layer propagation. This results in more extensive expansion of fractures within the upper and lower reservoirs while limiting the propagation within the target injection layer. At the viscosity of 300 mPa·s (Fig. 13d), hydraulic fractures exhibit relatively similar heights and widths across varying interlayer

thicknesses, indicating that under the viscosity condition of 300 mPa·s, the difference in the required injection volume for hydraulic fractures to pass through interlayers ranging from 6 to 12 m is relatively small.

Figure 14a shows the fracture geometric shape when the fracture length reaches 180 m under the condition of 10 mPa·s viscosity. Figure 14b–d is the fracture morphology of hydraulic fracture through the interlayers under different viscosity. Increasing viscosity makes fractures more likely to extend in the vertical direction, and the width of the fractures when crossing through interlayers increases with the increase in viscosity, while the fracture length decreases. When the viscosity increases from 100 to 300 mPa·s, the leak-off of the fracturing fluid in the rock formation decreases, resulting in a significant increase in fracture width. However, the reduction in fracture length upon crossing the interlayers is only
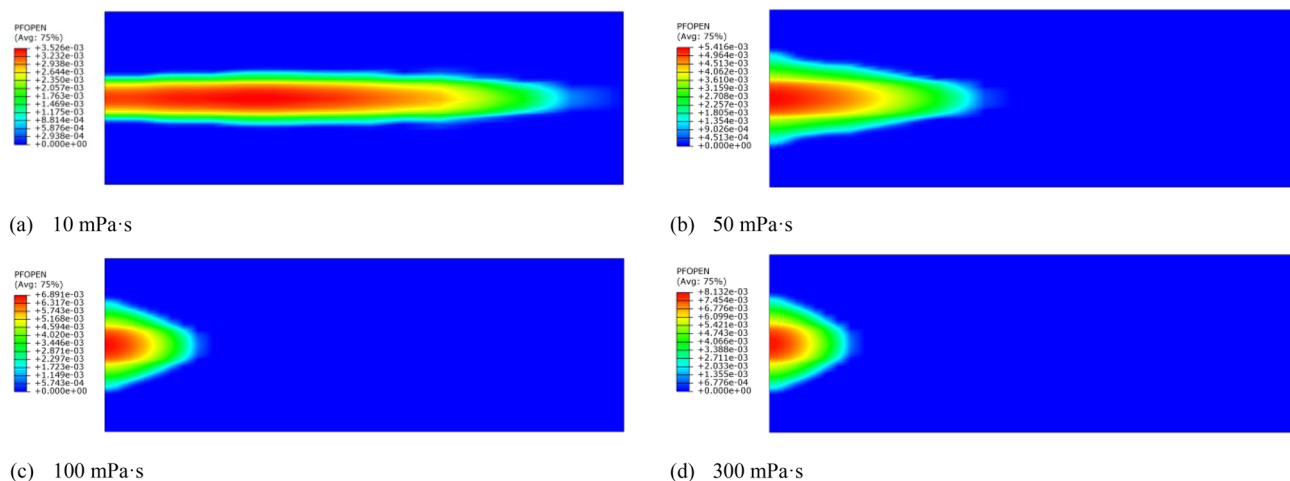
(a) 10 mPa·s

(b) 50 mPa·s

(c) 100 mPa·s

(d) 300 mPa·s

Fig. 14 The extensions of fracture length when the interlayer is 8 m under different viscosities

1.86 m, which is not a significant change in terms of fracture length extension. High-viscosity fracturing fluids can generate higher pressure within the fractures due to increased flow resistance in hydraulic fractures, making it easier to achieve cross-layer propagation. On the other hand, high-viscosity fracturing fluids cause hydraulic fractures to extend shorter distances in the fracture length direction, preventing the formation of long proppant-supported fractures. Therefore, in consideration of actual subsurface conditions, optimizing engineering parameters should involve simultaneous assessment of the varied impact of fracturing fluid viscosity on different aspects of hydraulic fractures.

5.3 Effect of the Minimum Horizontal Principal Stress Differential Between Layers on the Vertical Propagation of Hydraulic Fracture Through Interlayers

Based on the stress distribution variations in the sand–mud interbeds of the Es$_3$ reservoir, the minimum horizontal principal stress differential were set at − 4 MPa, − 2 MPa, 0 MPa, 2 MPa, and 4 MPa. The minimum horizontal principal stress differential between layers critically affects the ability of hydraulic fractures to pass through the interlayer. Typically, hydraulic fractures propagate in the direction perpendicular to the minimum horizontal principal stress (Zhou et al. 2019). The minimum horizontal principal stress directly influences the fracture width and can impact the extension of the fracture length and height.

Figure 15a–d depicts variations in hydraulic fracture width in different thickness interlayers under various stress conditions. When the minimum horizontal principal stress differentials are -4 MPa and -2 MPa, hydraulic fractures can vertically pass through the upper and lower interlayers of reservoir S2. However, once the fractures enter the S1 and S3 reservoirs, they encounter difficulties in further extending along the fracture length. Instead, there is a tendency for them to expand within the interlayers M2 and M3, resulting in the fracture width and length within the interlayers exceeding those within the reservoir. This leads to an excessive area of ineffective fracture propagation. When the minimum horizontal principal stress differential is 0 MPa, the minimum horizontal principal stress does not influence the expansion of fractures. At this point, variations in the mechanical properties of the formation rocks and other stress differences lead to changes in the fracture morphology at different layers. Under the 0 MPa stress differential, the curve depicting the variation of hydraulic fracture width with respect to height within interlayer thicknesses of 6–12 m gradually transitions from a trapezoidal shape to concave. This transition is attributed to the higher elastic modulus of the reservoir compared to the interlayer, causing the width of hydraulic fractures within the reservoir to gradually become smaller than those within the interlayer as the injection volume increases. With the minimum horizontal principal stress differential of 2 MPa, hydraulic fractures can propagate through interlayers with thicknesses of 6 m, 8 m, and 10 m but are unable to propagate through the 12 m interlayer. When the minimum horizontal principal stress differential is 4 MPa, fractures are completely confined within the reservoir, unable to achieve cross-layer propagation.

The increase in stress differential has a pronounced inhibitory effect on the height of hydraulic fractures. As evident from the longitudinal extension results of hydraulic fractures in Fig. 16, fractures exhibit a stronger tendency to propagate and expand in the direction of both width and length within rock layers with lower minimum horizontal principal stress. Smaller stress differentials make it easier for hydraulic fractures to achieve cross-layer propagation. However, when the stress differential is negative, the effective fracture area
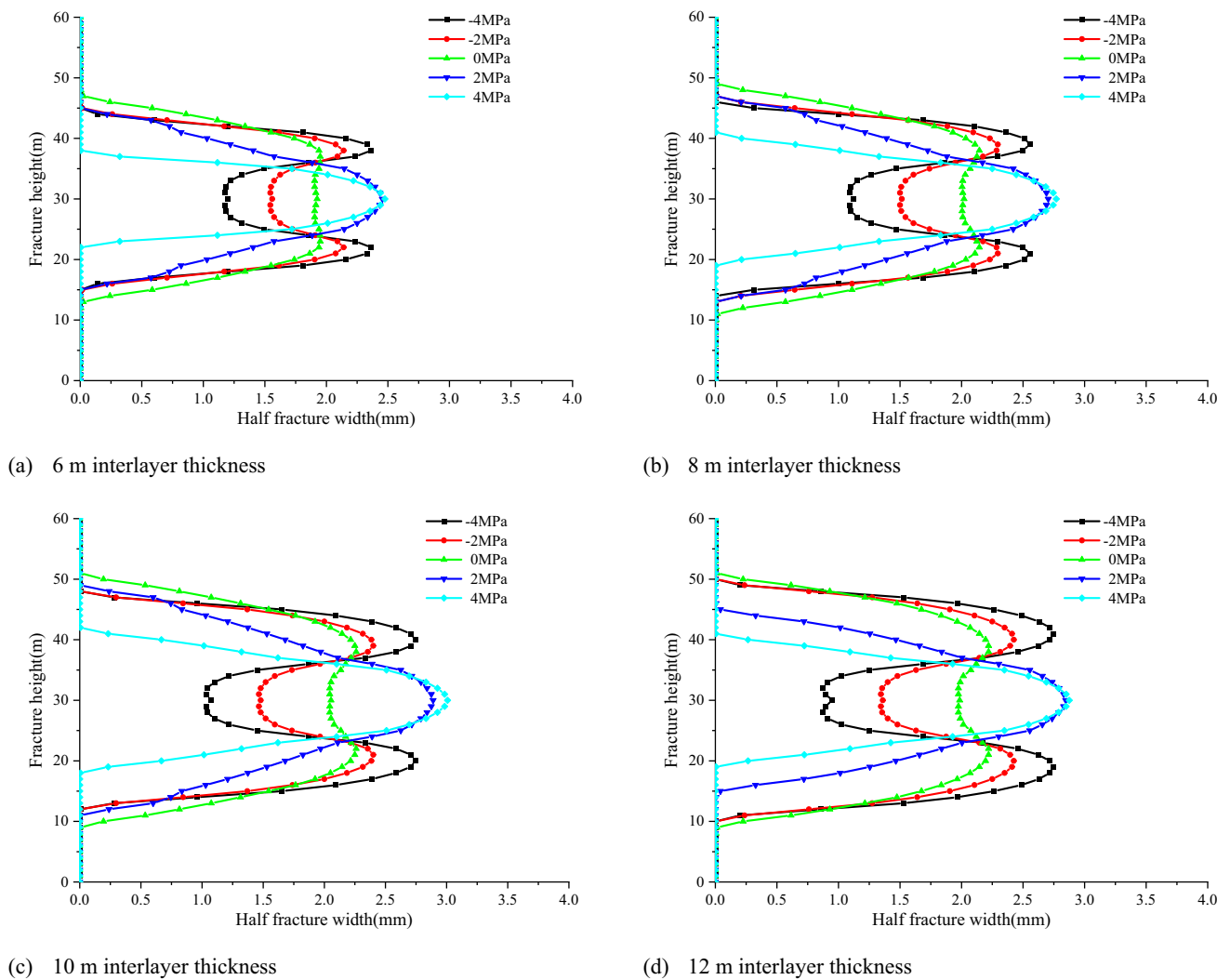
(a) 6 m interlayer thickness

(b) 8 m interlayer thickness

(c) 10 m interlayer thickness

(d) 12 m interlayer thickness

Fig. 15 The results of hydraulic fracture propagation through layers with varying the minimum horizontal principal stress differentials between layers under different interlayer thicknesses

experiences a significant reduction. Therefore, when selecting perforation intervals and hydraulic fracturing engineering parameters, it is crucial to ensure that hydraulic fractures extend as much as possible within the reservoir, while avoiding regions of lower interlayer stress.

5.4 Effect of Reservoir Thickness on the Vertical Propagation of Hydraulic Fracture Through Interlayers

The thickness of sandstone reservoirs and shale interlayers in the target formation varies alternately. Therefore, in this section, considering the thickness distribution range of the BZ25-1 Es$_3$ reservoir, four reservoir thicknesses were set at

10 m, 12 m, 14 m, and 16 m. It analyzes the vertical cross-layer propagation of hydraulic fractures under different reservoir and interlayer thickness conditions.

When the interlayer thickness is 6 m (Fig. 17a), hydraulic fractures in reservoirs with thicknesses of 16 m or less can propagate through the interlayer. Under the same injection volume, when hydraulic fractures in the 16 m reservoir pass through the interlayer, fractures in the 10–14 m reservoirs have already reached the boundaries of the interlayers M1 and M4 vertically. When the interlayer thickness is 8 m (Fig. 17b), hydraulic fractures in the 16 m reservoir cannot pass through the interlayer. Under the conditions of a 12 m reservoir, the width of hydraulic fractures in layers M2, S2, and M3 is slightly larger than the width of fractures under
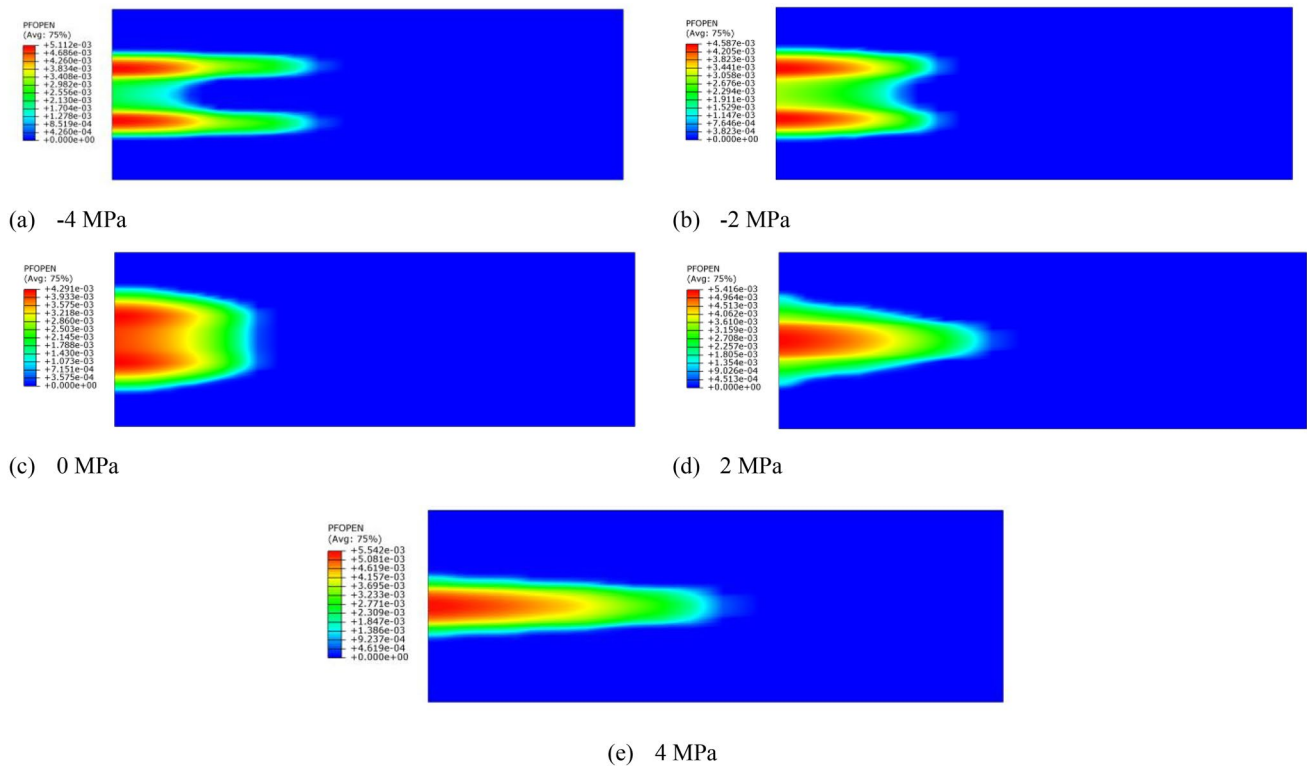
Fig. 16 The extensions of fracture length when the interlayer is 8 m under different stress differences

the conditions of a 10 m reservoir, while the width of fractures in S1 and S3 reservoirs is generally the same. When the interlayer thickness is 10 m (Fig. 17c), hydraulic fractures in both 10 m and 12 m reservoirs can propagate through the interlayer. Fractures in the 10 m reservoir have extended to the boundary interlayer and are constrained in height by it. When the interlayer thickness reaches 12 m (Fig. 17d), only hydraulic fractures in the 10 m reservoir thickness can propagate through the interlayer. The width of hydraulic fractures in the 12–16 m reservoir thickness decreases with an increase in reservoir thickness.

When the reservoir thickness is 10 m, the hydraulic fracture length within the reservoir is 55.03 m (Fig. 18a). With an increase in reservoir thickness to 12 m and 14 m (Fig. 18b and c), the corresponding hydraulic fracture lengths extend to 82.78 m and 138.2 m, respectively. The variation in fracture length indicates a significant enhancement in the propagation extent of hydraulic fractures within the reservoir as the thickness increases. At a reservoir thickness of 16 m (Fig. 18d), the hydraulic fracture becomes constrained by interlayers in the vertical direction and cannot pass through the interlayer. In comparison with the 12 m reservoir, the hydraulic fracture's overall width in the 10 m reservoir is smaller. This phenomenon is caused by the hydraulic fracture opening into the upper and lower reservoirs, which leads to fluid distribution into the S1 and S3 reservoirs.

Consequently, the pressure within the fracture in the S2 reservoir decreases, leading to fracture closure in S2 and a reduction in hydraulic fracture width.

6 Discussion

(1) The Es$_3$ sand–mud interbedded formations of BZ25-1 oilfield have low permeability, which belongs to medium-porosity, and low- to ultra-low-permeability reservoir. This formation is characterized by pronounced vertical heterogeneity, with significant variations in mechanical parameters. Longitudinal changes in the thickness of sandstone and mudstone layers contribute to uneven stress distribution, severely inhibiting the vertical expansion of hydraulic fractures. Consequently, reservoir development is challenging, and achieving the anticipated outcomes in hydraulic fracturing operations is difficult. To enhance the fracturing effectiveness of the formation, the Bozhong region will employ the offshore hydraulic fracturing vessels for hydraulic fracturing operations and reservoir modification. This study utilizes the finite element method to establish a three-dimensional fluid–solid coupling numerical model. Through this model, a simulation investigation is conducted on the vertical cross-layer propagation of hydraulic fractures within the sand–mud interbedded reservoir of the Es$_3$ formation

(a) 6 m interlayer thickness

(b) 8 m interlayer thickness

(c) 10 m interlayer thickness
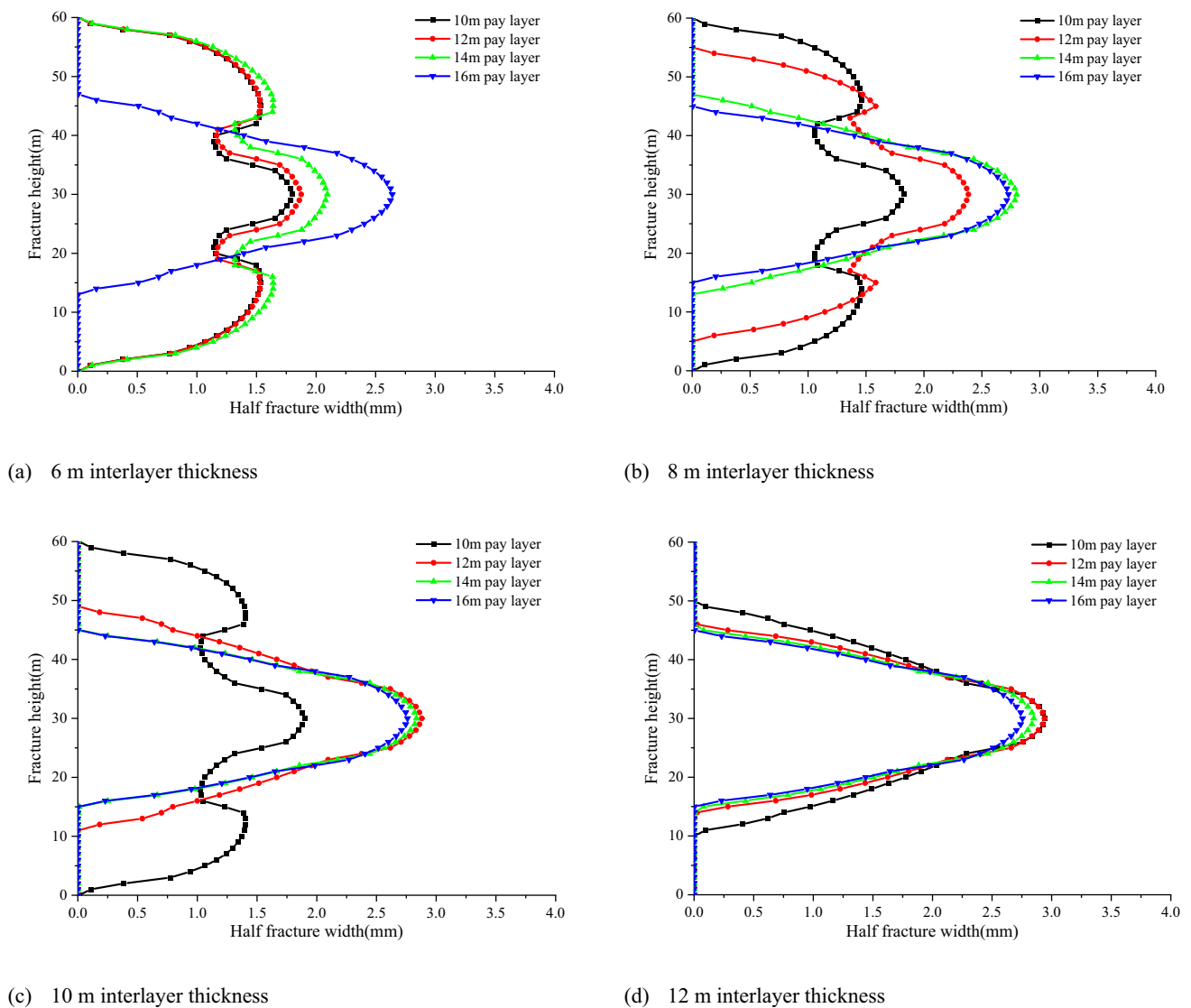
(d) 12 m interlayer thickness

Fig. 17 The results of hydraulic fracture propagation through layers with varying reservoir thicknesses under different interlayer thicknesses

in the BZ 25–1 oilfield, considering both engineering factors and stratigraphic conditions. Compared to other studies (Guo et al. 2017; Oyedokun and Schubert 2017), this paper systematically varies the interlayer thickness and explores the impact of interlayer thickness changes on the cross-layer propagation of hydraulic fractures. To illustrate the influence of alterations in engineering parameters and stratigraphic conditions on the effectiveness of hydraulic fractures cross-layer propagation, the injection situation of hydraulic fractures crossing the interlayer are summarized (Fig. 19). Due to the disparity between simulation and actual construction time, the ratio of fracturing fluid injection volumes is used to characterize result variations (with the minimum injection volume set to 1).

(2) Engineering factors significantly influence the extension of fractures. Increasing injection rate can provide

higher intra-fracture pressure for hydraulic fractures to propagate through thicker interlayers and effectively reduce the required injection volume for cross-layer propagation (Fig. 19a). When viscosity is low, fractures cannot propagate through the interlayers, and raising viscosity effectively reduces the leak-off of fracturing fluid, enhancing the tip penetration capability of hydraulic fractures (Fig. 19b). In the simulation results, under viscosity conditions of 100 mPa·s and 300 mPa·s, the required injection volumes for hydraulic fractures to pass through 6–12 m interlayers are close. Within the 12 m interlayer, the required injection volume for cross-layer propagation at 100 mPa·s is only 7.2% higher than that at 300 mPa·s. This indicates that, once a specific viscosity threshold is surpassed, there is no longer a significant change in the injection volume needed for hydraulic fracture passing through interlayers as
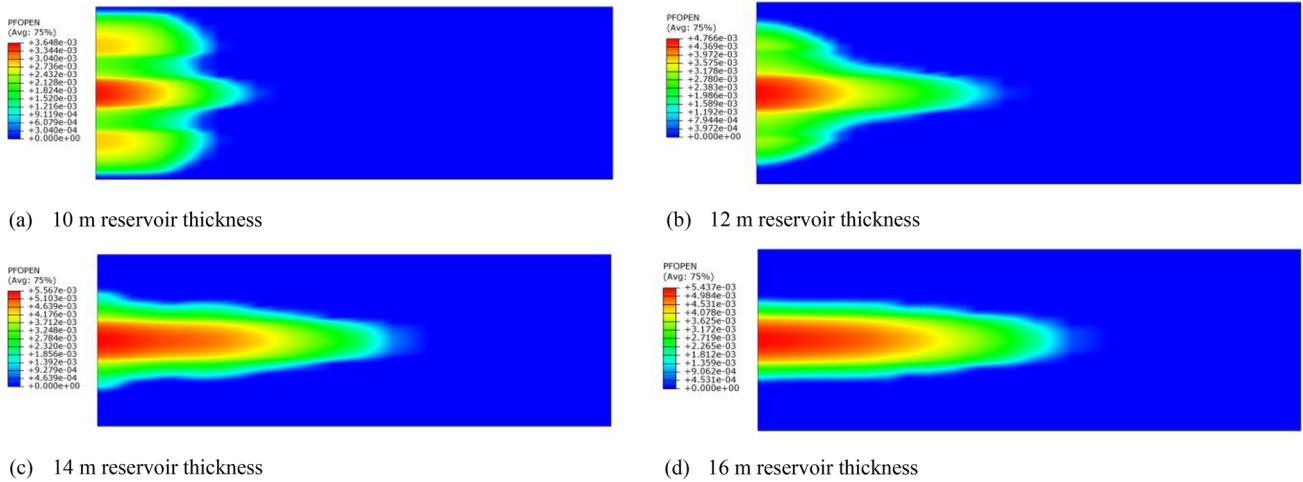
(a)   10 m reservoir thickness

(b)   12 m reservoir thickness

(c)   14 m reservoir thickness

(d)   16 m reservoir thickness

Fig. 18 The extensions of fracture length when the interlayer is 8 m under different reservoir thicknesses

(a)   Injection rate

(b)   Viscosity of fracturing fluid

(c) Minimum horizontal principal stress differentials between layers
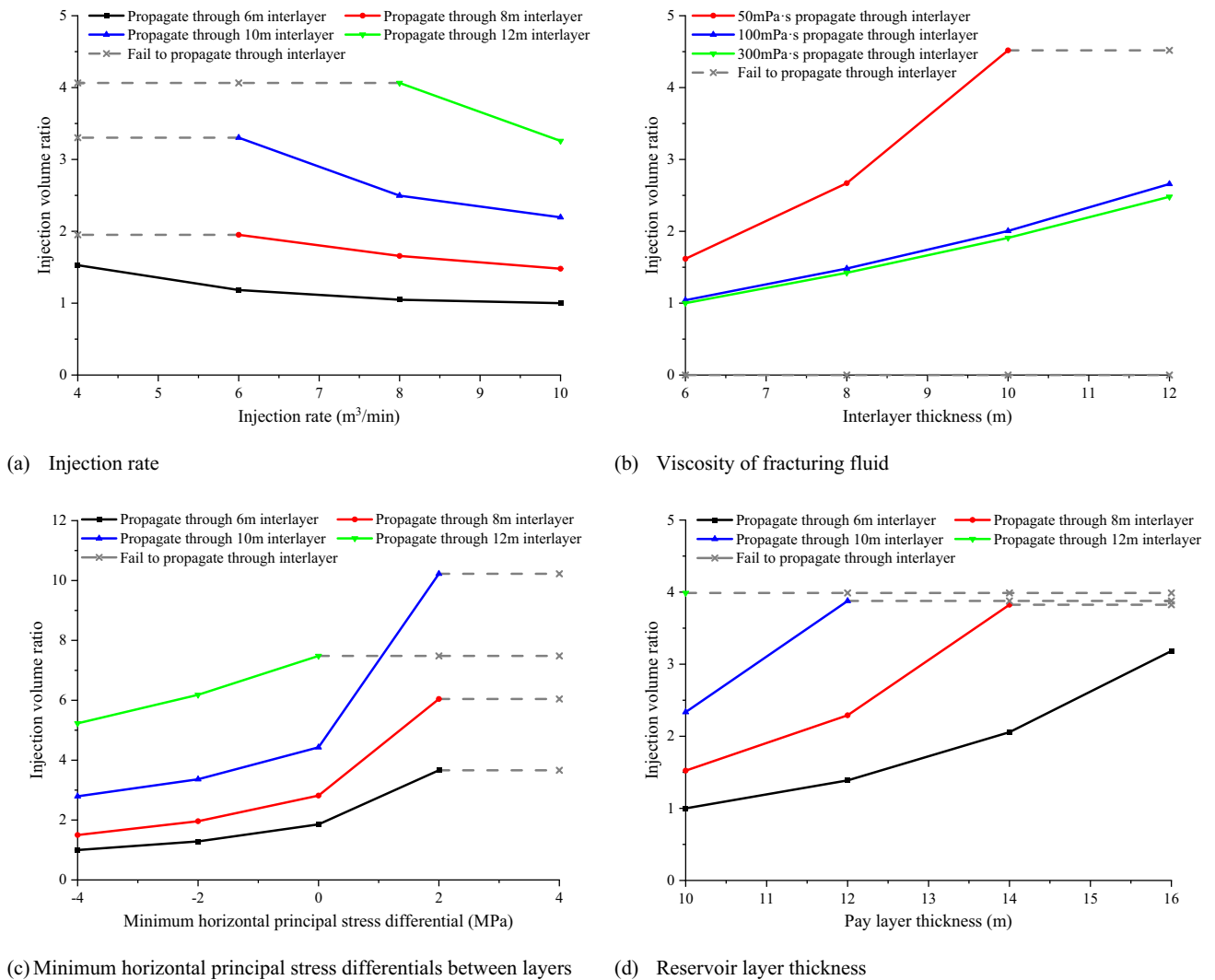
(d)   Reservoir layer thickness

Fig. 19 The ratio of liquid injection volume when hydraulic fractures propagate through the interlayer under different conditions

the viscosity continues to increase. This is mainly because the leak-off of the fracturing fluid in the formation changes slightly. The offshore hydraulic fracturing vessels enhance the pumping capacity of offshore oilfield fracturing operations. However, the fracturing operations parameters of " large injection rate and high viscosity " are easy to cause the hydraulic fracture to propagate through the layer too fast, thus affecting the fracture length extension in the reservoir. Therefore, for the target fractured reservoir section, small injection rate and low viscosity can be used for fracturing to extend the hydraulic fracture in the direction of fracture length. Then, large pumping rate or high-viscosity liquid for injecting to achieve cross-layer propagation. This approach aims to optimize hydraulic fracture extension within the reservoir, augmenting the distribution area of hydraulic fractures and thereby enhancing overall production.

(3) Geological conditions exert a great influence on the effectiveness of hydraulic fracture in passing through interlayers. The minimum horizontal principal stress differential between reservoir and interlayer is the most critical factor affecting the vertical propagation efficiency of hydraulic fractures through interlayers. As the stress differential increases from 0 to 2 MPa, there is a steep rise in the required injection volume for hydraulic fracture cross-layer propagation (Fig. 19c). When the stress difference increases to 4 MPa, the hydraulic fracture has been completely unable to pass through the barrier. When the horizontal stress of the mudstone layer exceeds that in of the sandstone layer, the fracture height is suppressed, making it challenging to achieve cross-layer propagation. Conversely, when the horizontal stress in the mudstone layer is less than that in the sandstone layer, the hydraulic fracture tends to propagate within the mudstone layer, resulting in an excessive area of ineffective fractures. This partially explains the observed lower-than-expected production improvement following hydraulic fracturing operations on-site. From Fig. 19d, it can be observed that there is a positive correlation between the increase in reservoir thickness and the escalation trend in the required injection volume for fracture propagating through interlayers. The increase in reservoir thickness gradually confines hydraulic fractures within the reservoir. The smaller the reservoir thickness, the smaller the area occupied by fractures within the reservoir, the higher the fracture height, the easier it is to extend into the interlayer, the greater the energy carried by the fracture tip, and the easier it is to achieve the effectiveness of propagating through the interlayer. The increase of the interlayer thickness leads to the excessive extension of the hydraulic fracture in the direction of the fracture length. After the fracture area increases, the pressure in the fracture cannot provide enough energy for the fracture tip, resulting in the failure of the hydraulic fracture to propagate through the interlayer vertically. Spanning more strata should be the main goal of fracturing

(Wan et al. 2019). To achieve cross-layer propagation and ensure the expansion and extension of fractures within the production layer, the perforation location should be selected according to the stress difference of different strata and the thickness distribution of the sand–mud interbeds, and avoid the high stress barrier as much as possible. In thick reservoirs, fracturing with small injection rate or low viscosity is recommended to control hydraulic fractures' extension predominantly in the direction of fracture length, facilitating better acquisition of effective fracture area and improving the effectiveness of fracturing treatments.

7 Conclusion

Aiming at the sand–mud interbed reservoir of the third member of Shahejie Formation in Bozhong 25–1, this paper studies the cross-layer propagation of hydraulic fractures under different mudstone interlayer thickness conditions from two aspects of engineering factors and geological parameters by establishing three-dimensional fracture propagation numerical models. The main conclusions of the simulation are as follows:

1. Compared with large injection rate, the use of low injection rate will lead to hydraulic fracture tending to extend along the direction of fracture length. When the same injection volume of fracturing fluid is used, increasing the injection rate benefits hydraulic fracture to propagate through the interlayer. The variable injection rate fracturing method of 'large injection rate propagate through interlayer and low injection rate extend fracture' can be used to enhance reservoir productivity.

2. The use of low viscosity fracturing fluid will make it difficult for hydraulic fracture to enter the interlayer. Increasing the viscosity can significantly improve the vertical propagation effect of hydraulic fracture, widen the fracture, but the fracture extension length will be significantly reduced. The viscosity combination method of 'high viscosity + low viscosity' can be used to optimize the fracturing effect.

3. The minimum horizontal principal stress differential between the reservoir and the interlayer has a very important influence on the cross-layer propagation results of hydraulic fracture, and the change of stress difference will directly affect the fracture propagation morphology. When the minimum horizontal principal stress of the layers is the same, the extension of the hydraulic fracture in the direction of fracture height and fracture length is more uniform.

4. The increase of reservoir thickness will result in hydraulic fracture requiring a greater liquid injection volume to extend to the interlayer, thereby increasing the exten-

sion degree of fracture in the length inside the reservoir, leading to an increase in fracture area and a decrease in fracture tip energy, which in turn affects the vertical propagation outcomes of hydraulic fractures.

5. In order to realize the cross-layer propagation of sand–mud interbed reservoirs with different interlayer thicknesses, it is necessary to first select the layer with the minimum horizontal principal stress and the most suitable reservoir thickness for perforation, and then configure reasonable fracturing fluid viscosity and injection rate for fracturing construction.

Declaration

Conflict of interest The authors declare that they have no conflict of interest.

References

Adachi JI, Detournay E, Peirce AP (2010) Analysis of the classical pseudo-3D model for hydraulic fracture with equilibrium height growth across stress barriers. Int J Rock Mech Min 47(4):625–639

Benzeggagh ML, Kenane MJCS (1996) Measurement of mixed-mode delamination fracture toughness of unidirectional glassepoxy composites with mixed-mode bending apparatus. Compos Sci Technol 56(4):439–449

Chen Z (2012) Finite element modelling of viscosity-dominated hydraulic fractures. J Pet Sci Eng 88:136–144

Chitrala Y, Moreno C, Sondergeld C, Rai C (2013) An experimental investigation into hydraulic fracture propagation under different applied stresses in tight sands using acoustic emissions. J Petrol Sci Eng 108:151–161

Dahi Taleghani A, Gonzalez M, Shojaei A (2016) Overview of numerical models for interactions between hydraulic fractures and natural fractures: challenges and limitations. Comput Geotech 71:361–368

Fan BT, Chen ZR, Jiang H, Wu Y, Li B, Yang Q, Li L (2021) Status and prospect of fracturing technology for CNOOC unconventional and offshore low permeability reservoirs. 33(04):112-119

Fisher K, Warpinski N (2012) Hydraulic-fracture-height growth: real data. Spe Prod Oper 27(01):8–19

Fu HF, Cai B, Geng M, Jia AL, Weng DW, Liang TC, Zhang FS, Wen XY, Xiu NL (2022a) Three-dimensional simulation of hydraulic fracture propagation based on vertical reservoir heterogeneity. Nat Gas Ind 42(5):56–68

Fu SH, Hou B, Xia Y, Chen M, Wang S, Tan P (2022b) The study of hydraulic fracture height growth in coal measure shale strata with complex geologic characteristics. J Petrol Sci Eng 211:110164

Gu H, Siebrits E (2008) Effect of formation modulus contrast on hydraulic fracture height containment. SPE Prod Oper 23(02):170–176

Guo JC, Luo B, Lu C, Lai J, Ren JC (2017) Numerical investigation of hydraulic fracture propagation in a layered reservoir using the cohesive zone method. Eng Fract Mech 186:195–207

Haddad M, Sepehrnoori K (2015) Simulation of hydraulic fracturing in quasi-brittle shale formations using characterized cohesive layer: stimulation controlling factors. J Unconvent Oil Gas Resources 9:65–83

Huang BX, Liu JW (2017) Experimental investigation of the effect of bedding planes on hydraulic fracturing under true triaxial stress. Rock Mech Rock Eng 50(10):2627–2643

Huang CH, Zhu HY, Wang JD, Han J, Zhou GQ, Tang XH (2022) A Fem-Dfn model for the interaction and propagation of multi-cluster fractures during variable fluid-viscosity injection in layered shale oil reservoir. Petrol Sci 19(6):2796–2809

Huang J, Ma XD, Shahri M, Safari R, Yue KM, Mutlu U (2016) Hydraulic Fracture Growth and Containment Design in Unconventional Reservoirs. Arma Us Rock Mechanics/Geomechanics Symposium ARMA-2016–2412

Jeffrey Jr RG, Brynes RP, Lynch PJ, Ling DJ (1992) An Analysis of Hydraulic Fracture and Mineback Data for a Treatment in the German Creek Coal Seam. SPE Rocky Mountain Petroleum Technology Conference/Low-Permeability Reservoirs Symposium SPE-24362-MS

Jia AL, Wei YS, Guo Z, Wang GT, Meng DW, Huang SQ (2022) Development status and prospect of tight sandstone gas in China. Nat Gas Ind 42(1):83–92

Khisamitov I, Meschke G (2018) Variational approach to interface element modeling of brittle fracture propagation. Comput Method Appl M 328:452–476

Lu C, Li M, Guo JC, Tang XH, Zhu HY, Wang YH, Liang H (2015) Engineering geological characteristics and the hydraulic fracture propagation mechanism of the sand-shale interbedded formation in the Xu5 reservoir. J Geophys Eng 12(3):321–339

Oyedokun O, Schubert J (2017) A quick and energy consistent analytical method for predicting hydraulic fracture propagation through heterogeneous layered media and formations with natural fractures: the use of an effective fracture toughness. J Nat Gas Sci Eng 44:351–364

Pandey VJ, Rasouli V (2021) Vertical Growth of Hydraulic Fractures in Layered Formations. Spe Hydraulic Fracturing Technology Conference and Exhibition. OnePetro SPE-204155-MS

Shel E (2017) Influence of the Elastic Moduli Contrast on the Height Growth of a Hydraulic Fracture. Spe Russian Petroleum Technology Conference. OnePetro SPE-187834-MS

Simonson ER, Abou-Sayed AS, Clifton RJ (1978) Containment of massive hydraulic fractures. Soc Petrol Eng J 18(01):27–32

Song MS, Liu HM, Wang Y, Liu YL (2020) Enrichment rules and exploration practices of Paleogene shale oil in Jiyang Depression, Bohai Bay Basin. China Petrol Explor Dev 47(2):225–235

Sun LD, Zou CN, Jia AL, Wei YS, Zhu RK, Wu ST, Guo Z (2019) Development characteristics and orientation of tight oil and gas in China. Petrol Explor Dev 46(6):1015–1026

Tang XH, Zhu HY, Li KD (2023) A FEM-DFN-based complex fracture staggered propagation model for hydralic fracturing of shale gas reservoirs. Nat Gas Ind 43(1):162–176

Teufel LW, Clark JA (1984) Hydraulic fracture propagation in layered rock: experimental studies of fracture containment. Soc Petrol Eng J 24(01):19–32

Tomar V, Zhai J, Zhou M (2004) Bounds for element size in a variable stiffness cohesive finite element model. Int J Numer Methods Eng 61(11):1894–1920

Van Eekelen HAM (1982) Hydraulic fracture geometry: fracture containment in layered formations. Soc Petrol Eng J 22(3):341–349

Wan L, Hou B, Tan P, Chang Z, Muhadasi Y (2019) Observing the effects of transition zone properties on fracture vertical propagation behavior for coal measure strata. J Struct Geol 126:69–82

Wang Y, Wang XJ, Song GQ, Liu HM, Zhu DS, Zhu DY, Ding JH, Yang WQ, Yin Y (2016) Genetic connection between mud shale lithofacies and shale oil enrichment in Jiyang Depression. Bohai Bay Basin Petrol Explor Dev 43(5):696–704

Wang YL, Hou B, Wang D, Jia ZH (2021) Features of fracture height propagation in cross-layer fracturing of shale oil reservoirs. Petrol Explor Dev 48(2):402–410

Warpinski NR, Clark JA, Schmidt RA, Huddle CW (1981) Laboratory Investigation on the Effect of in Situ Stresses on Hydraulic Fracture Containment//Denver, CO: Soc. Pet. Eng. AIME: 55–66.

Warpinski NR, Schmidt RA, Northrop DA (1982) In-situ stresses; the predominant influence on hydraulic fracture containment. J Petrol Technol 34(3):653–664

Wei YS, Jia AL, He DB, Wang JL, Han PL, Jin YQ (2017) Comparative analysis of development characteristics and technologies between shale gas and tight gas in China. Nat Gas Ind 37(11):43–52

Wu R, Deng JG, Wei BH, Liu W, Li Y, Li M, Peng CY (2017) Numerical modeling of hydraulic fracture containment of tight gas reservoir in Shihezi Formation, Linxing Block. J China Coal Soc 42(09):2393–2401

Xu D, Hu RL, Gao W, Jia JG (2015) Effects of laminated structure on hydraulic fracture propagation in shale. Petrol Explor Dev 42(4):523–528

Xu WY, Prioul R, Berard T, Weng XW, Kresse O (2019) Barriers to hydraulic fracture height growth: A new model for sliding interfaces. Spe Hydraulic Fracturing Technology Conference and Exhibition. OnePetro SPE-194327-MS

Xu XQ, Tao L, Wang H (2022) Study on vertical multifracture propagationsin deep shale reservoir with natural fracture network. Energy Sci Eng 10(8):2892–2908

Yang ZZ, Zhang D, Yi LP, Li XG, Li Y (2021) Longitudinal propagation model of hydraulic fracture and numerical simulation in multi-layer superimposed coalbed. J China Coal Soc 46:3268–3277

Yue K, Olson JE, Schultz RA (2019) The effect of layered modulus on hydraulic-fracture modeling and fracture-height containment. Spe Drill Completion 34(04):356–371

Zhang FS, Wu JF, Huang HY, Wang XH, Luo HR, Yue WH, Hou B (2021) Technological parameter optimization for improving the complexity of hydraulic fractures in deep shale reservoirs. Nat Gas Ind 41(1):125–135

Zhang J, Xie ZG, Pan YS, Tang JZ, Li YW (2023) Synchronous vertical propagation mechanism of multiple hydraulic fractures in shale oil formations interlayered with thin sandstone. J Petrol Sci Eng 220:111229

Zhao HF, Wang XH, Liu ZY, Yan YJ, Yang HX (2018) Investigation on the hydraulic fracture propagation of multilayers-commingled fracturing in coal measures. J Petrol Sci Eng 167:774–784

Zhou L, Su XP, Lu YY, Ge ZL, Zhang ZY, Shen ZH (2019) A new three-dimensional numerical model based on the equivalent continuum method to simulate hydraulic fracture propagation in an underground coal mine. Rock Mech Rock Eng 52(8):2871–2887

Zhou W, Shi GX, Wang JB, Liu JT, Xu N, Liu PY (2022) The influence of bedding planes on tensile fracture propagation in shale and tight sandstone. Rock Mech Rock Eng 55(3):1111–1124

Zhu HY, Huang CH, Tang XH, Mclennan JD (2023) Multicluster Fractures Propagation During Temporary Plugging Fracturing in Naturally Fractured Reservoirs Integrated with Dynamic Perforation Erosion. Spe J: 1–17

Zhu HY, Jin XC, Guo JC, An FC, Wang YH (2016) Coupled flow, stress and damage modelling of interactions between hydraulic fractures and natural fractures in shale gas reservoirs. Int J Oil Gas Coal Technol 4:359–390

Zhu HY, Zhao X, Guo JC, Jin XC, An FC, Wang YH, Lai XD (2015) Coupled Flow-stress-damage simulation of deviated-wellbore fracturing in hard-rock. J Nat Gas Sci Eng 26:711–724

Authors and Affiliations

Xu Guo[1,2] · Haiyan Zhu[1,2] · Peng Zhao[3] · Hu Jiang[4] · Guangai Wu[4] · Lei Tao[1,2] · Chao Liu[1,2] · Shijie Chen[1,2] · Jinghua Chen[1,2]

✉ Haiyan Zhu
zhuhaiyan040129@163.com

[1] State Key Laboratory of Oil & Gas Reservoir Geology and Exploitation, Chengdu University of Technology, Chengdu 610059, Sichuan, China

[2] College of Energy, Chengdu University of Technology, Chengdu 610059, Sichuan, China

[3] State Key Laboratory of Geohazard Prevention and Geoenvironment Protection, Chengdu University of Technology, Chengdu 610059, Sichuan, China

[4] CNOOC Research Institute, Beijing 100027, China